Adhesion failure mechanism of asphalt-aggregate interface under an extreme saline environment: A molecular dynamics study

Yingxue Zou[a], Yangming Gao[b], Anqi Chen[a,*], Shaopeng Wu[a,**], Yuanyuan Li[c], Haiqin Xu[a], Huan Wang[a], Ye Yang[c], Serji Amirkhanian[d]

[a] State Key Laboratory of Silicate Materials for Architectures, Wuhan University of Technology, Luoshi Road 122, Wuhan 430070, China; zouyingxue@whut.edu.cn (Y. Zou); xuhaiqin@whut.edu.cn (H. Xu); 303561@whut.edu.cn (H. Wang)

[b] School of Civil Engineering and Built Environment, Liverpool John Moores University, Byrom Street, Liverpool L3 3AF, UK; y.gao@ljmu.ac.uk (Y. Gao)

[c] School of Civil Engineering and Architecture, Wuhan Institute of Technology, Wuhan 430074, China; liyy@wit.edu.cn (Y. Li); yangye@stu.wit.edu.cn (Y. Yang)

[d] Department of Civil Construction and Environmental Engineering, University of Alabama, Tuscaloosa, AL 35487, USA; samirkhanian@eng.ua.edu (S. Amirkhanian)

*Correspondence: anqi.chen@whut.edu.cn (A. Chen)

**Correspondence: wusp@whut.edu.cn (S. Wu)

Graphical abstract:

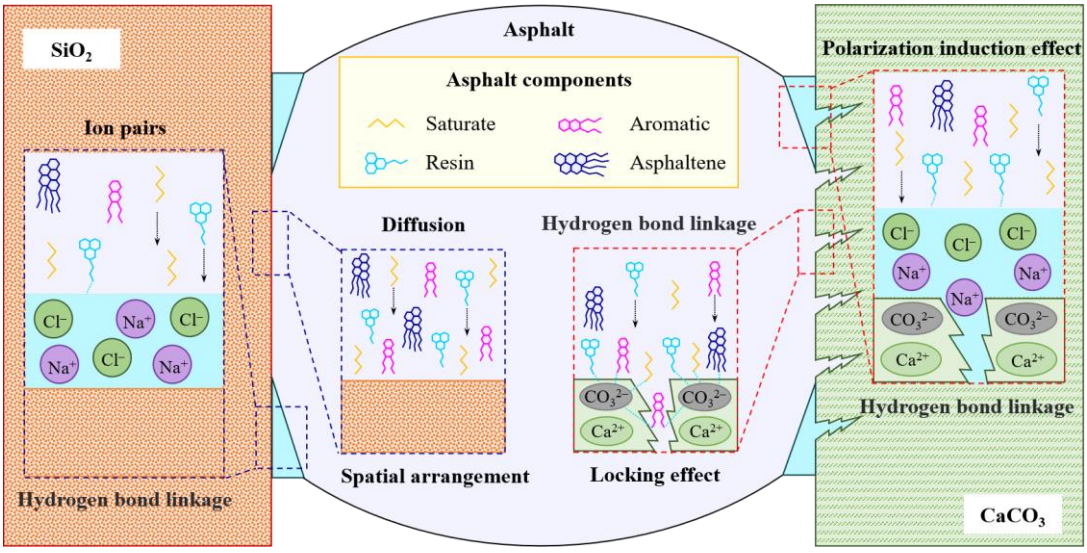

ABSTRACT

The extreme saline environment seriously threatens the service life of asphalt pavement. The interface adhesion failure between asphalt and aggregate is fundamental to pavement diseases. Therefore, the interface of asphalt-NaCl solution-mineral was simulated by molecular dynamics to investigate the adhesion failure mechanism between asphalt and aggregate in an extremely saline environment. The results show that the polarization-inducing effects of sodium and chloride ions promote the cross-

sectional diffusion of the NaCl solution at the interfaces and contribute to the redistribution and rediffusion of asphalt components, and the formation of hydrogen bonds between water and asphalt components. The NaCl solution prevents the accumulation of saturates, resins, and asphaltenes on the SiO_2 surface, and strips aromatics from the SiO_2 surface due to the interaction. Sodium ions can be attracted to the oxygen atoms on CO_3^{2-} to occupy active sites on the $CaCO_3$ than asphalt, which makes it easier for chloride ions to penetrate the asphalt molecule and asphalt components to detach from $CaCO_3$. These behaviors effectively impair the adhesion at the asphalt-mineral interface. The 3 wt% and 20 wt% NaCl solutions have the greatest effect on the adhesion work of the asphalt-SiO_2 and asphalt-$CaCO_3$, reducing them by 55.93 % and 66.03 %, respectively.

Keywords: asphalt-aggregate interface; adhesion failure; saline environment; damage mechanism; molecular dynamics

1. Introduction

Asphalt pavement refers to the road surface structure formed by blending and compacting aggregate materials with asphalt as the binder [1]. It is currently the most widely used road surface structure owing to its excellent engineering properties and economic efficiency, such as high durability, low noise, and driving comfort [2]. During service, the water on the road surface penetrates the asphalt mixture under the action of load, resulting in the cohesion failure of the asphalt binder and the adhesion failure between the asphalt binder and aggregate [3, 4]. It leads to water damage to pavement, which is manifested as loosening, pothole, and deformation, directly reducing the service life and threatening the traffic safety of asphalt pavement [5, 6]. As two main components of asphalt mixture, the adhesive force between asphalt binder and aggregate is much weaker than the internal cohesion of asphalt binder [7]. Aggregate is polar and hydrophilic, the asphalt adhering to aggregate surface adhesion is easy to be replaced by polar moisture, forming a three-layer system of asphalt [8]. Therefore, understanding the mechanism of adhesion failure between asphalt and aggregate is crucial to the sustainable development strategy of the

pavement industry.

Serious water damage diseases generally occur in these areas, including coastal areas, saline areas, and high-freezing areas [9, 10]. Salt spray and tides, which often occur in coastal areas, can carry salt from seawater into asphalt pavements [11]. With a total area of 5 million hectares of saline soils in the humid southeastern coastal region, rainwater can carry large amounts of salt solution onto asphalt pavements [12]. In frozen areas, ice melts salt and salt storage asphalt binder is used as the traditional means of snow and ice melting on asphalt pavements [13]. Seawater, saline-alkali soil, snowmelt salt, and salt storage asphalt binder all contain high levels of NaCl that have a certain harm to the service life of asphalt pavement [14]. The effects of dynamic water, temperature, freeze-thaw cycles, wet and dry cycles, loading, and UV irradiation on the performance of asphalt mixtures in chloride salt environments have been studied by scholars. The results show that dynamic water accelerates the erosion of chlorinated salt on asphalt mixtures, and it is related to the concentration and temperature of the salt solution [15]. The destruction of asphalt mixture voids can be caused by crystallization pressure and freezing expansion pressure of salt solution under the coupled action of sea spray and freeze-thaw cycles [16]. Loading and dynamic water have the greatest effect on pavement performance, followed by chloride concentration and temperature, and UV radiation had a lesser effect [17]. The resistance to salt damage of the asphalt mixture is also depend on the adhesion between asphalt binder and aggregate, which rely on the physicochemical interaction on the interfaces [18]. Xu et al. [19] found that the adhesion work of asphalt binder with aggregate decreased significantly with the addition of salt through contact angle tests and boiling water tests. Zhang et al. [20] conducted an atomic force microscopy (AFM) test and a four-component test on asphalt binders in a NaCl environment. The results showed that the NaCl solution altered the chemical composition content of the asphalt binder and weakened the adhesion of the asphalt binder to aggregate. Yang et al. [21] compared the asphalt-aggregate adhesion property after salt erosion through the surface free energy. They found that the salt solution increased the polarity component and

decreased the dispersion component, which reduces the asphalt-aggregate adhesion work. However, laboratory characterizations can only reflect changes in performance after erosion, making it challenging to visualize the evolution mechanism for the chemical components and adhesion of the asphalt-aggregate interface in a salt environment.

Molecular dynamics (MD) simulation is a computational method that simulates the behavior of molecules at the microscopic level based on the principles of Newtonian mechanics [22]. In the field of materials science, MD simulations have been applied to study the mechanical characteristics and chemical reactions of materials [23, 24]. It can be used to simulate interfacial adhesion failures and quantify the mechanisms at the molecular scale. Long et al [25] combined AFM tests and MD simulations to find that chloride ions lead to the formation of a gradient zone with weak adhesion on the asphalt surface, and assist water molecules to penetrate the softened asphalt film to reach the asphalt-aggregate interface, thereby eroding its interfacial adhesion. However, the impact of sodium chloride on the interfacial adhesion based on the molecular scale is less well studied. And NaCl concentration in the environment varies with different regions (offshore and offshore) and atmospheric humidity. The law and mechanism of adhesion failure at the interface in extreme NaCl concentration are still unclear. In addition, it can be found from the relevant research that the conclusions based on adhesion properties are often relatively dispersive. The reason is that the chemical composition, structural morphology, and mechanical properties at the interface need to be further refined.

Herein, the impact of extreme concentrations of NaCl solution on the adhesion of asphalt binder to the mineral interface and the damage mechanisms are investigated in this study. Common minerals in the aggregate are quartz and calcite, which are the most abundant components of the acidic and basic minerals respectively [26, 27]. MD simulations of the interface of asphalt binder on silica and calcium carbonate substrates were undertaken in an environment with extreme concentrations of NaCl. The characterizations contain the diffusion behavior of the NaCl solution at the interface, the spatial

arrangement of asphalt components, and the changes in the interfacial adhesion work.

2. Simulation models and methods from molecular dynamics

2.1. Mineral model

Natural rock minerals are polycrystalline and have a local periodicity [28]. The geometric structure of minerals is usually represented by a box with parallel sides [29]. Quartz and calcite were selected and the effect of NaCl solution on their adhesion to asphalt binder was investigated by MD simulation. Table 1 showed the structures and the detailed parameters of the minerals from the Cambridge Structural Databas. The qualitative analysis of interfacial adhesion is not significantly affected by different Miller planes [30]. According to the previous papers and the principle of the most stable energy and the minimum lattice mismatch, the most suitable Miller planes were selected to present sufficient coordination sites for asphalt adhesion [26]. Taking SiO_2 as an example, the construction of the supercell model was illustrated in Fig. 1a. The unit cell was cut along the Miller index surface (1,0,0) and then constructed into a supercell with a thickness of 20.65 Å, which met the requirement of greater than the cutoff radius of 15.5 Å. Next, a vacuum layer was placed on top of the supercell to form a mineral block with three-dimensional periodic boundary conditions. The movement of the mineral was avoided by constraining the bottom of the supercell within half the thickness of the mineral slab, which satisfied a balance between computational efficiency and accuracy. And the mineral surface was allowed to relax sufficiently to adsorb with the asphalt molecules. Similarly, the Miller index surface (0,1,8) with a thickness of 22.02 Å was chosen to be constructed into a $CaCO_3$ supercell, also following the principle that the mineral thickness was greater than the cutoff radius.

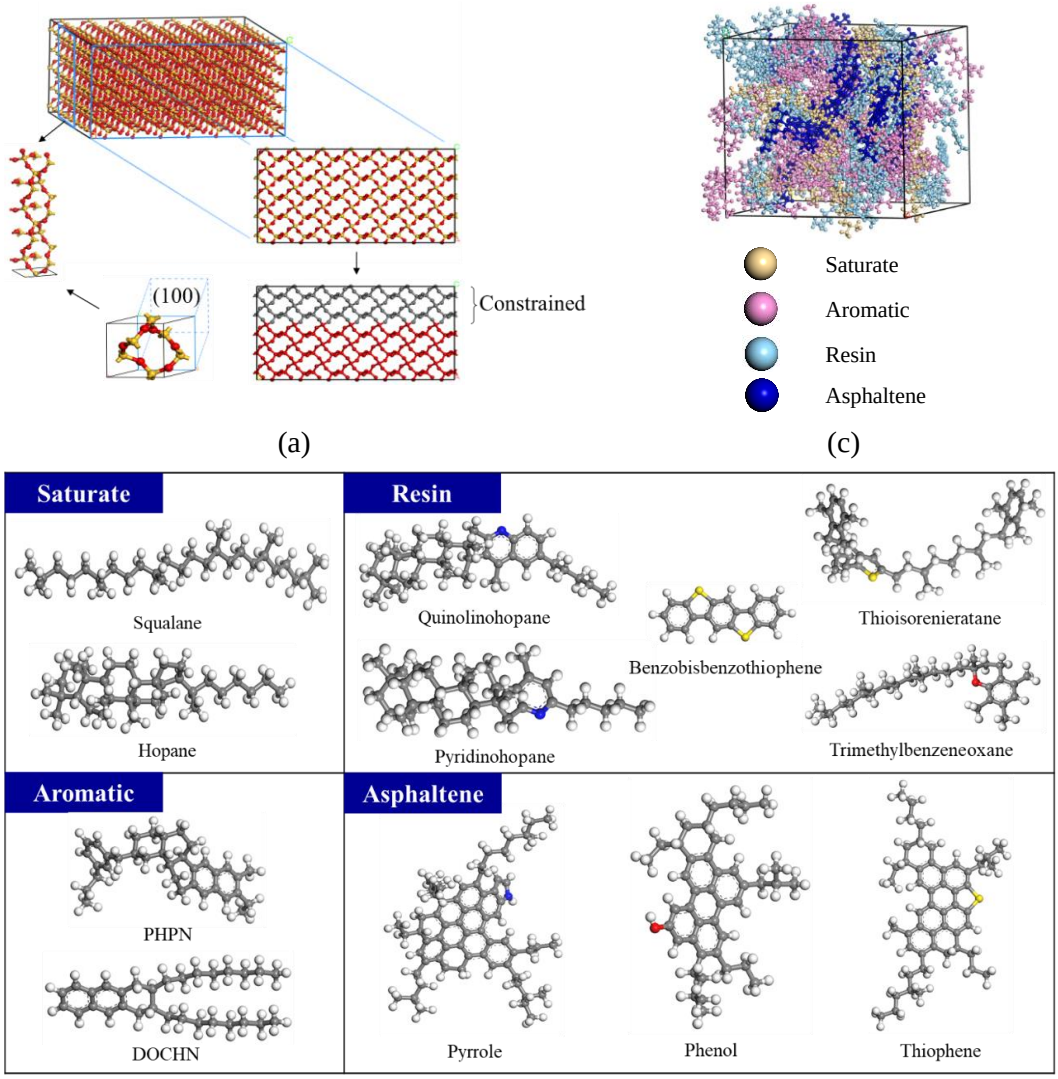

Fig. 1. Molecular models for interface system (gray atom is carbon, white atom is hydrogen, red atom is oxygen, yellow atom is sulfur, and blue atom is nitrogen); (a) construction of supercell model for SiO_2 mineral; (b) 12-component of asphalt model; (c) molecular model of asphalt binder.

Table 1

Detailed parameters of minerals (yellow and red represent silicon atoms and oxygen atoms, respectively; green and grey represent calcium atoms and carbon atoms, respectively).

Chemical formula	Unit cell structure	Lattice parameters	Miller planes	Supercell size (Å × Å × Å)
SiO_2	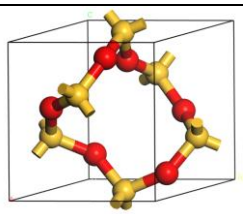	a=b=4.913 Å, c=5.405 Å; α=β=90°, γ=120°	(1,0,0)	39.30 × 37.83 × 20.65
$CaCO_3$	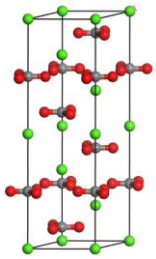	a=b=4.990 Å, c=17.061 Å; α=β=90°, γ=120°	(0,1,8)	39.92 × 38.55 × 22.02

2.2. Asphalt model

The molecule structures of the 12 components from the AAA-1 asphalt model were selected illustrated in Fig. 1b [31]. Based on the ratio of component molecules in the AAA-1 model shown in Table 2, an asphalt model with an initial density of 0.1 g/cm^3 under three-dimensional cycling conditions was constructed using the amorphous cell module in Materials Studio software [32]. The geometric optimization process with 5000 iterations was performed to eliminate unreasonable configurations in the model so that the energy of each molecule leveled off when the system reached minimum energy. MD simulations were performed using a constant molecular number, volume, and temperature (NVT) ensemble at 298 K with a time step of 1 fs for 100 ps [33]. It was then further equilibrated in the isothermal-isobaric (NPT) ensemble at 298 K and 1.0 atm for 100 ps to obtain a stable structure with a stable density. The system was maintained near a certain temperature and pressure within the Andersen barostat and Nose-Hoover-Langevin thermostat. After dynamic equilibrium, the density of the asphalt model was finally stabilized at 0.997 g/cm^3. Herein, a confined layer of asphalt model with a density of

0.997 g/cm^3 was created by using the amorphous cell module. The width and length of which are set to the same as the mineral model to enable the construction of asphalt-mineral layers, which were performed by the geometry optimization and NVT ensemble for 100 ps, and the confined layer of asphalt as shown in Fig. 1c. The force field of COMPASS was applied to allows accurate calculation and prediction [34]. And the atom-based summation method and Ewald summation method were applied to calculate the electrostatic interaction and the van der Waals interaction with a cutoff distance of 15.5 Å, respectively [35].

Table 2

Molecular compositions of virgin asphalt models [31].

Component	Molecular	Chemical formula	Number of molecular	Mass fraction (%)
Saturate	Squalene	$C_{30}H_{62}$	4	10.71
	Hopane	$C_{35}H_{62}$	4	
Aromatic	PHPN	$C_{35}H_{44}$	11	30.72
	DOCHN	$C_{30}H_{46}$	13	
Resin	Quinolinohopane	$C_{40}H_{59}N$	4	41.95
	Thioisorenieratane	$C_{40}H_{60}S$	4	
	Benzobisbenzothiophene	$C_{18}H_{10}S_2$	15	
	Pyridinohopane	$C_{36}H_{57}N$	4	
	Trimethylbenzeneoxane	$C_{29}H_{50}O$	5	
Asphaltene	Phenol	$C_{42}H_{54}O$	3	16.62
	Pyrrole	$C_{66}H_{81}N$	2	
	Thiophene	$C_{51}H_{62}S$	3	

2.3. MD simulations

The system model of the asphalt-mineral interface was created by combining a mineral block with an asphalt layer. Then the mirror interactions were avoided by adding a 30 Å vacuum slab above the asphalt model, which was 2 times the cutoff radius. The asphalt-0% NaCl-mineral interfacial model was formed by placing 200 water molecules at the interface between asphalt and mineral. This number of

151 water molecules was chosen because it can provide an adequate solvated environment without making
152 the system too large and drastically increasing the computational cost. And so on, different NaCl solutions
153 were formed by adding different numbers of sodium and chloride ions. Coastal pavements are generally
154 exposed to salt spray, which typically has a concentration of 0.7 mg/m^3 or less [36]. With the deposition
155 of salt in the salt spray and splashing of seawater, the concentration of salt environment on the pavement
156 can reach the concentration of seawater, which is 3% [37]. Thus, for asphalt pavements, long-term
157 exposure to seawater concentrations can also be defined as an extreme salt environment. Additionally,
158 the NaCl concentration in seawater is about 3 wt%, and the NaCl concentration often used in the
159 laboratory for salt-erosion acceleration experiments is 10 wt%, and 20 wt% is a more extreme
160 concentration of NaCl solution [14]. Hence, the salt environment was set to 3 wt%, 10 wt%, and 20 wt%
161 NaCl solution. Taking the SiO_2 mineral as an example, the interface systems were illustrated in Fig. 2a
162 to 2e. Based on molar mass and density, the 10 wt % NaCl solution layer contains 200 water molecules,
163 7 sodium ions, 7 chloride ions, and so on for other concentrations of NaCl solutions. After geometry
164 optimization, the interface systems of asphalt-mineral without and with 0%, 3%, 10%, and 20% NaCl
165 solution were subjected to NVT ensemble for 300ps at 298K.

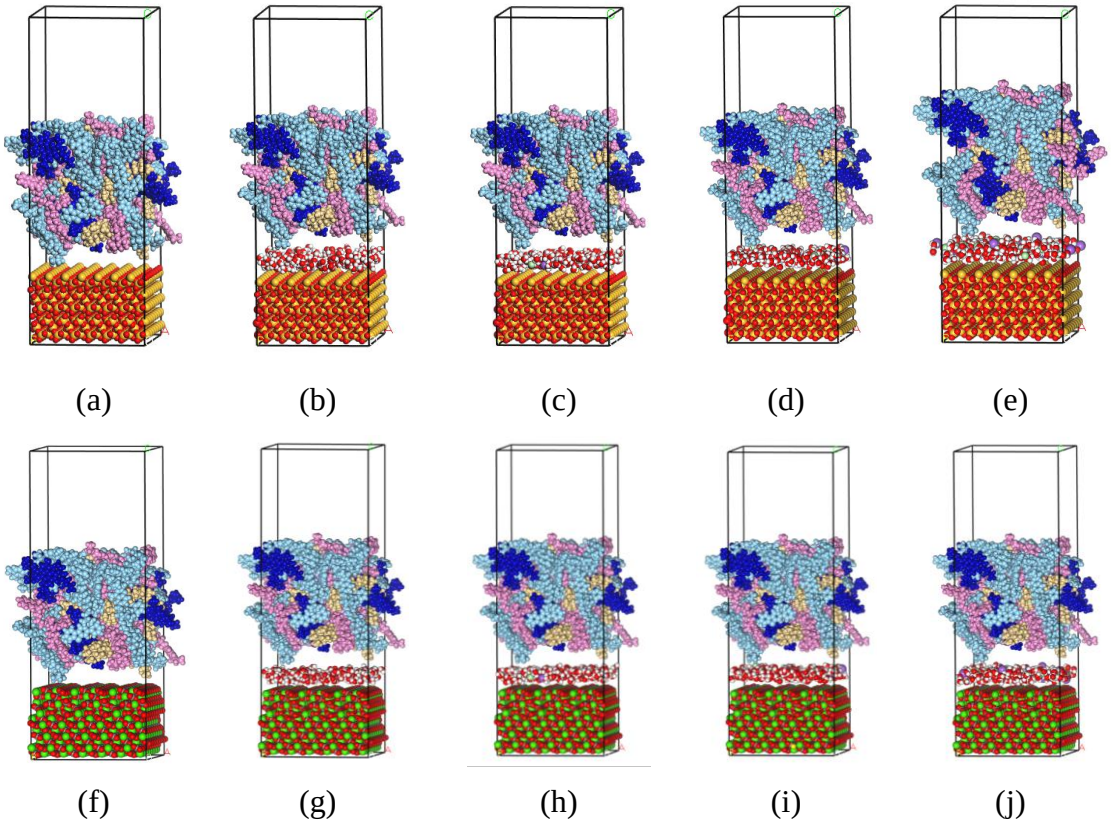

Fig. 2. Interface system model (purple and green represent sodium and chloride ions, respectively); (a) asphalt-SiO_2; (b) asphalt-0% NaCl solution-SiO_2; (c) asphalt-3% NaCl solution-SiO_2; (d) asphalt-10% NaCl solution-SiO_2; (e) asphalt-20% NaCl solution-SiO_2; (f) asphalt-$CaCO_3$; (g) asphalt-0% NaCl solution-$CaCO_3$; (h) asphalt-3% NaCl solution-$CaCO_3$; (i) asphalt-10% NaCl solution-$CaCO_3$; (j) asphalt-20% NaCl solution-$CaCO_3$.

3. Results and conclusions

3.1. Verification of asphalt model

Density is the fundamental thermodynamic parameter of asphalt binder, and stable density values of asphalt models can be obtained after molecular dynamics simulations of asphalt models under the NPT ensemble [38]. After dynamic equilibrium, the density of the asphalt model was stabilized at 0.997 g/cm^3, which was closer to the actual density shown in Table 3. Cohesive energy density (CED) and solubility parameter (δ) can evaluate the intermolecular attraction and compatibility of asphalt [39]. The CED is the cohesive energy per unit of volume, the square root of which is the δ. The calculation formulas of the two are shown in Eq. (1) and (2).

$$CED = \frac{E_{coh}}{V} = -\frac{\langle E_{inter} \rangle}{V} = \frac{\langle E_{intra} \rangle - \langle E_{total} \rangle}{V} \quad (1)$$

$$\delta = \sqrt{CED} \quad (2)$$

Where E_{coh} and V represent the cohesion and occupied volume of the asphalt model, E_{inter} represents the interaction energy, E_{intra} is the intramolecular energy, and E_{total} is the total energy of the system. The brackets $\langle \cdots \rangle$ is an average over the NVT ensemble. The calculated results are shown in Table 3, which are within the test values. Therefore, these parameters validate the reliability of the asphalt model.

Table 3

Validation parameters of asphalt model.

Parameters	Calculated values	Experiment value
Density (298.15K, g/cm^3)	0.997	1.01–1.04 [40]
CED (10^8 J/m^3)	3.22	3.19–3.32 [41]
δ ((J/cm^3)$^{0.5}$)	17.95	13.30–22.50 [42]

3.2. Appearance of the interfacial system in the NaCl environment

The asphalt-SiO_2 and asphalt-$CaCO_3$ systems after MD simulation are compared under dry conditions and NaCl solution conditions to observe the interfacial adhesion state, as shown in Fig. 3. After MD simulation, the SiO_2 bound by covalent bonds remains regular and flat, and the asphalt is flatly distributed on the SiO_2 surface at dry. While water molecules and asphalt interpenetrate to isolate the asphalt from the SiO_2 at 0% NaCl solution, and the interfacial separation is slightly weakened by 3% NaCl. An embedded locking phenomenon is observed at the asphalt-$CaCO_3$ interface, this is because ionic bonds in $CaCO_3$ bonded by ionic bonds are more likely to adsorb asphalt molecules. That is consistent with the Scanning electron microscope results in the previous study [43]. Whereas the presence of water fills these depressions debonding asphalt from $CaCO_3$, and the appearance of the asphalt-$CaCO_3$ interface can be insignificantly affected by 3% NaCl. The interface appearances under different NaCl concentrations are not discussed, because NaCl concentrations in the same interfacial system do not differ significantly in appearance.

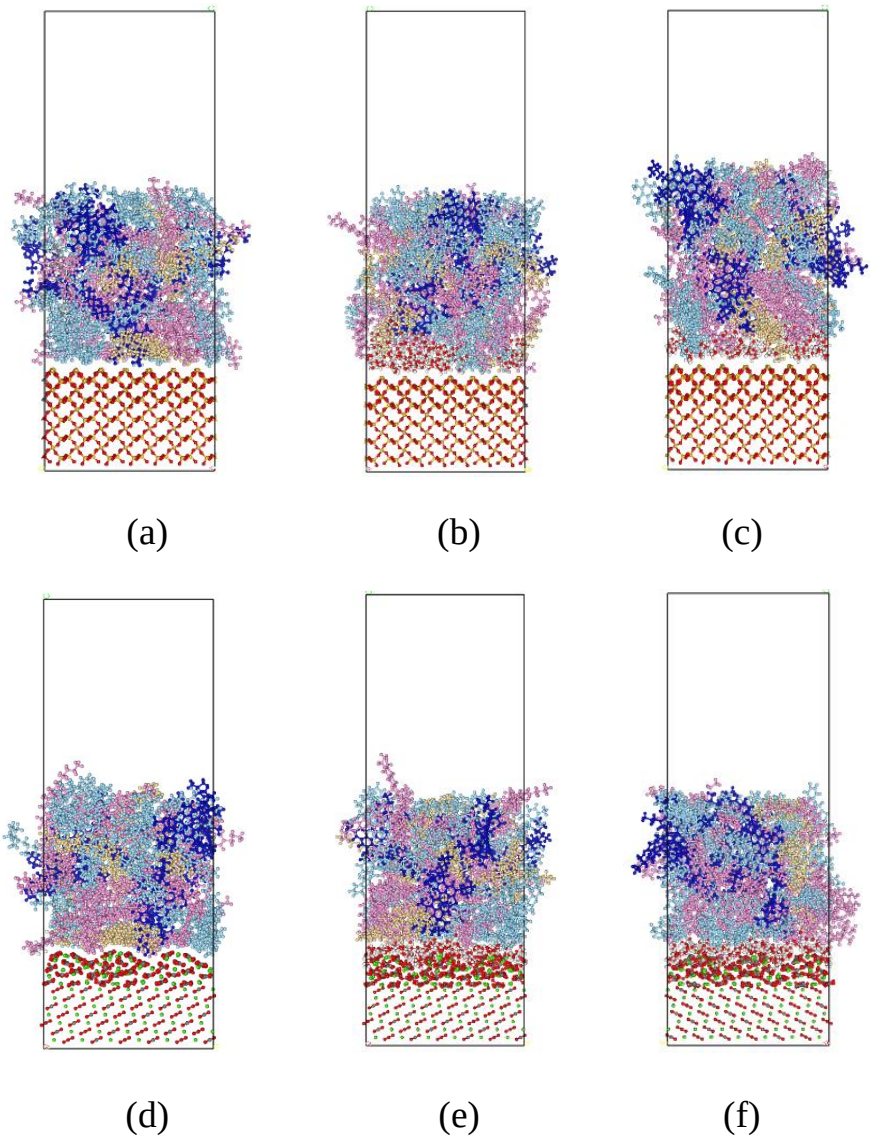

Fig. 3. Asphalt-mineral systems after adhesion simulations; (a) asphalt-SiO_2; (b) asphalt-0% NaCl solution-SiO_2; (c) asphalt-3% NaCl solution-SiO_2; (d) asphalt-$CaCO_3$; (e) asphalt-0% NaCl solution-$CaCO_3$; (f) asphalt-3% NaCl solution-$CaCO_3$.

3.3. Diffusion and distribution of NaCl solution at the asphalt-mineral interface

3.3.1. Diffusion coefficient of NaCl solution

The mean square displacement (MSD) function is employed to quantize the motion properties of molecules and ions and is an important parameter in molecular dynamics analysis, defined as the square of the displacement of a particle in a fixed period, expressed by Eq. (3) [44].

$$MSD = r^2(t) = \frac{1}{N}\left(\sum_{i=1}^{N} |r_i(t) - r_i(0)|^2\right) \quad (3)$$

where $r_i(0)$ and $r_i(t)$ are the position of molecule or ion i at the initial moment and time t; N is the number

of molecules or ions. To investigate the diffusion law of NaCl solution, the diffusion coefficient (D) from 200 to 300 ps during dynamic equilibrium is calculated using anisotropic displacement curves (including cross-sectional and lengthwise displacement curves) as well as isotropic displacement curves by Eq. (4) [45].

$$D = \frac{r^2(t)}{6t} \tag{4}$$

where *r(t)* is the molecular and ionic displacement.

Therefore, the D of NaCl solution is calculated by its MSD according to Eq. (4), and the curve of D with NaCl concentration is depicted in Fig. 4a and 4b. The isotropic D of the NaCl solution in the asphalt-SiO_2 system is dominated by the cross-sectional diffusion while the lengthwise D is almost zero. The cross-sectional D can be accelerated by low concentrations of NaCl, while that can be reduced to a lower D than 0% NaCl solution by high concentrations of NaCl. For the asphalt-$CaCO_3$ system, NaCl has a positive impact on the cross-sectional diffusion of the aqueous solution, and there is a peak in its effect at 3% NaCl. The NaCl accelerates the lengthwise D to a small extent and does not vary with the NaCl concentration. Therefore, the isotropic D of 3% NaCl solution is the highest, which is 1.47 times and 2.49 times that of 0% NaCl solution in the asphalt-SiO_2 system and asphalt-$CaCO_3$ system, respectively. The lengthwise diffusion of NaCl solution into the mineral interior is limited by the poor wettability between the solution and the minerals [46].

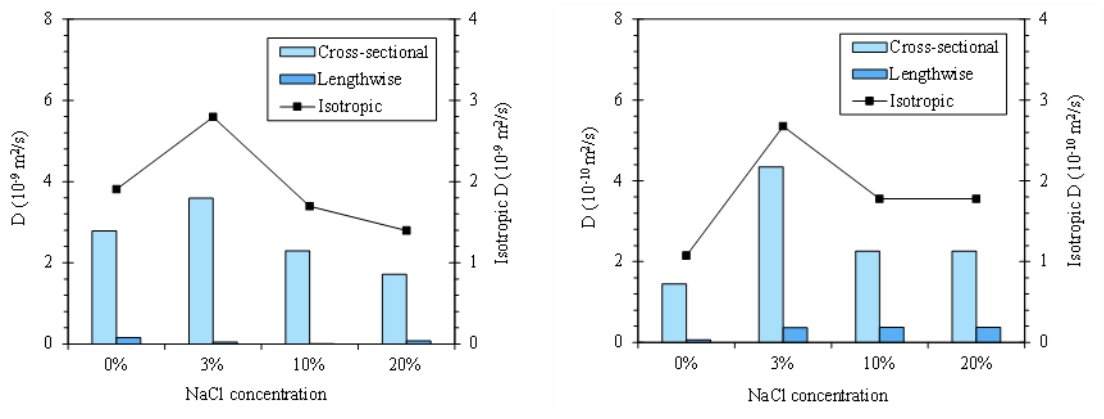

Fig. 4. Diffusion coefficient of NaCl solution; (a) asphalt-SiO_2; (b) asphalt-$CaCO_3$.

3.3.2. Performance parameters of NaCl solution

To further explore the diffusion behavior of NaCl solution at the interface, the performance parameters of NaCl solution are studied, including the radius of gyration (R_g) and fractional free volume (FFV) of NaCl solution. The R_g characterizes the stiffness of the NaCl solution, which affects the diffusion, and is calculated as in Eq. (5) [47].

$$R_g^2 = \frac{\sum m_i r_i^2}{\sum m_i} \tag{5}$$

where m_i and r_i are the mass and the radius of atom i, respectively. The FFV was employed to quantify the volume percentage of the NaCl solution that is not occupied by molecules [48]. It is calculated by Eq. (6).

$$FFV = \frac{V_{free}}{V_{free} + V_{occupied}} \times 100\% \tag{6}$$

where V_{free} and $V_{occupied}$ are the free volume and occupied volume, respectively. The results are illustrated in Fig. 5a and 5b. The R_g decreases with increasing NaCl concentration. NaCl exists in solution as the contact ion pairs and the solvent ion pairs, and the motion of atoms in solution is limited. That also leads to a decrease in the free volume of the atoms, and although the increase in atoms causes an increase in the occupied volume, the FFV still decreases. These are the reasons for the decrease in the D of the NaCl solution.

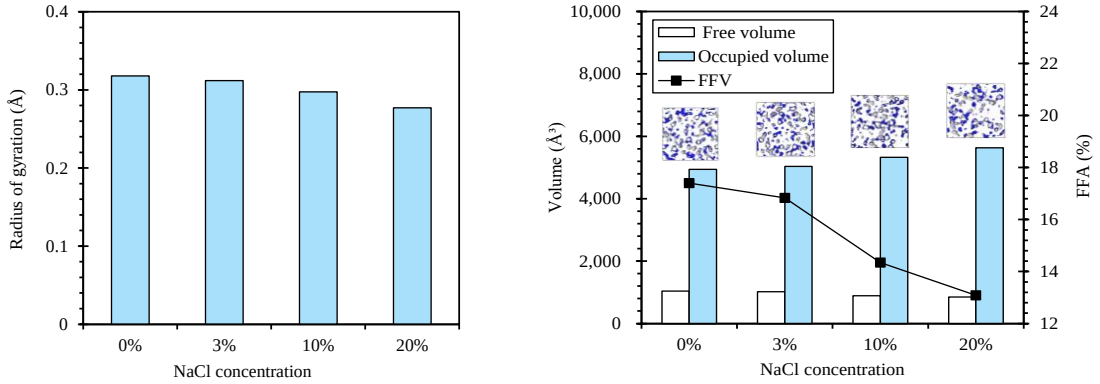

(a) (b)

Fig. 5. Performance parameters of NaCl solution; (a) and (b) radius of gyration and volume performance parameters.

3.3.3. Distribution of NaCl solution

After dynamic equilibrium, the cross-sectional distribution of the NaCl solution is characterized to observe the aggregation of aqueous solution, as shown in Fig. 6. The water molecules in 0% NaCl solution are not uniformly distributed at the SiO_2 interface, tending to agglomerate. The presence of 3% NaCl allows the water molecules to be more evenly distributed at the interface. This might be explained by the fact that ions promote the agglomeration of water molecules on the asphalt, due to the greater polarity than water molecules [49]. As the NaCl concentration increases, the aqueous solution is promoted to agglomerate at the interface [50]. And the water molecules are already evenly distributed on $CaCO_3$ at 0% NaCl solution. And there is no significant change in the distribution of water molecules with NaCl concentration.

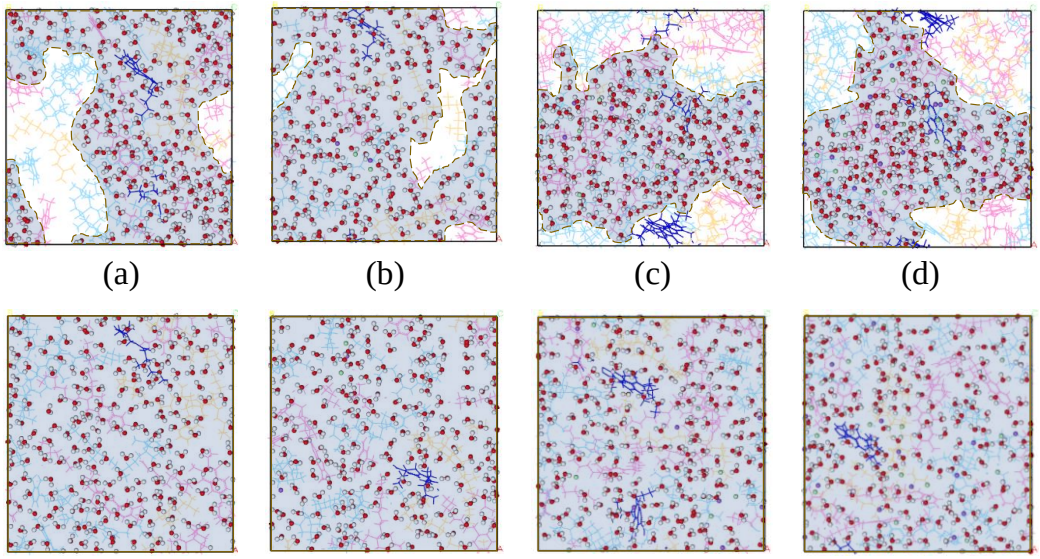

Fig. 6. Cross-sectional distribution of NaCl solution at the interfaces (the light blue areas represent areas where the aqueous solution accumulates; the display style of the asphalt components is line, saturates are yellow, aromatics are pink, resins are light blue, asphaltenes are dark blue); (a) asphalt-0% NaCl solution-SiO_2; (b) asphalt-3% NaCl solution-SiO_2; (c) asphalt-10% NaCl solution-SiO_2; (d) asphalt-20% NaCl solution-SiO_2; (e) asphalt-0% NaCl solution-$CaCO_3$; (f) asphalt-3% NaCl solution-$CaCO_3$; (g) asphalt-10% NaCl solution-$CaCO_3$; (h) asphalt-20% NaCl solution-$CaCO_3$.

The lengthwise distribution of molecules at the interfaces is used to observe the lengthwise diffusion

263 results of the NaCl solution, as illustrated in Fig. 7. Comparing the asphalt-SiO_2 system and asphalt-
264 $CaCO_3$ system at dry, the hydrogen bonds between asphalt components with $CaCO_3$ are found. Hydrogen
265 bonding is an electrostatic connection between electronegative atoms and hydrogen atoms, the presence
266 of which can strengthen the adhesion between them [51]. And NaCl is beneficial to the formation of
267 hydrogen bonds between water molecules and asphalt components. This may be due to the polarity
268 induction effect of increased polarity of NaCl solution on asphalt components. It can be observed from
269 Fig. 7 that the distribution of sodium and chloride ions present certain rules, so their mass densities
270 toward lengthwise direction are quantitatively calculated, as illustrated in Fig. 8. In the asphalt-SiO_2
271 system, the sodium ions mainly accumulate on the SiO_2 surface, and diffuse to the asphalt molecules to
272 a certain extent. Chloride ions also accumulate mainly on the SiO_2 surface, but the red area indicates that
273 chloride ions diffuse more easily to asphalt than sodium ions. This might be explained by the fact that
274 metal ions are more inclined to agglomerate on the surface of minerals, while chloride ions are
275 nucleophilic ions, the polarization induction effect of which makes them more inclined to approach
276 positively charged atoms in asphalt [52]. In asphalt-$CaCO_3$, the accumulation of sodium ions on $CaCO_3$
277 is more obvious, while the tendency of chloride ions to be attracted by asphalt is also more obvious. This
278 might be explained by the fact that sodium ions can be attracted by the negatively charged oxygen atom
279 on CO_3^{2-}, it is easier to occupy the active site on the surface of $CaCO_3$ and indirectly promote the diffusion
280 of chloride ions to asphalt.

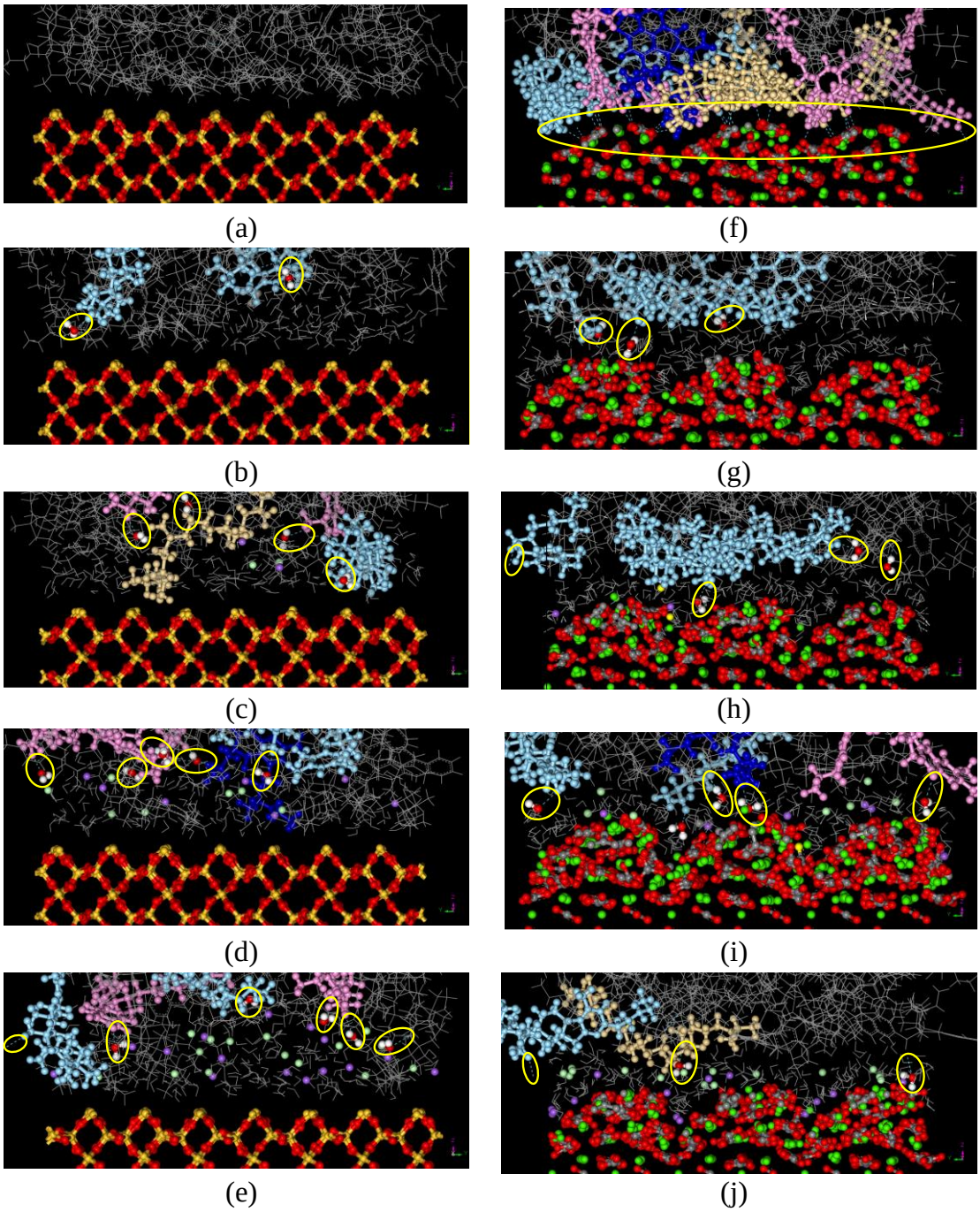

Fig. 7. Lengthwise distribution of molecules at the interfaces (blue dashed line represents hydrogen bonds that were circled by yellow thread, grey lines represent asphalt components that are not hydrogen bonded to water or mineral); (a) asphalt-SiO_2; (b) asphalt-0% NaCl solution-SiO_2; (c) asphalt-3% NaCl solution-SiO_2; (d) asphalt-10% NaCl solution-SiO_2; (e) asphalt-20% NaCl solution-SiO_2; (f) asphalt-$CaCO_3$; (g) asphalt-0% NaCl solution-$CaCO_3$; (h) asphalt-3% NaCl solution-$CaCO_3$; (i) asphalt-10% NaCl solution-$CaCO_3$; (j) asphalt-20% NaCl solution-$CaCO_3$.

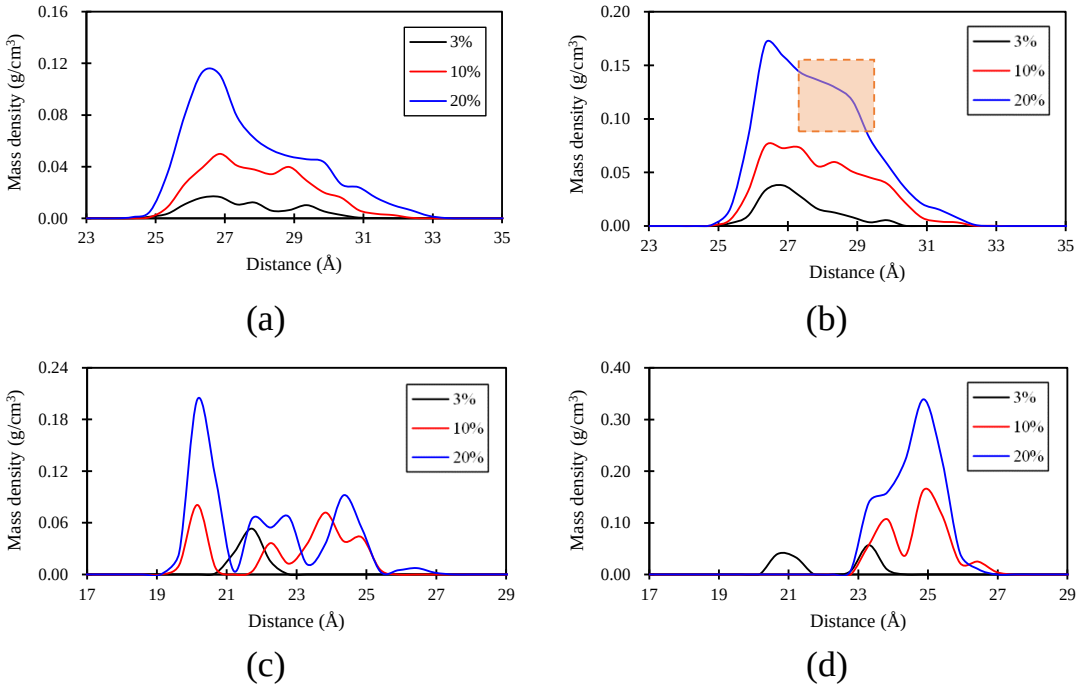

Fig. 8. Mass density of sodium and chloride ions towards the lengthwise direction; (a) sodium ions in the asphalt-SiO_2 system; (b) chloride ions in the asphalt-SiO_2 system; (c) sodium ions in the asphalt-$CaCO_3$ system; (d) chloride ions in the asphalt-$CaCO_3$ system.

3.4. Spatial arrangement of interfacial molecules at the interface in the NaCl environment

3.4.1. Distribution of NaCl solution and asphalt molecules

The spatial arrangement of interfacial molecules plays an important function in adhesion properties, and the lengthwise distribution of asphalt molecules and NaCl solution is plotted in Fig. 9. At dry, the asphalt agglomerates at 25-30 Å in the asphalt-SiO_2 system, manifesting asphalt agglomerates at the interface due to the interaction energy. However, NaCl prevents asphalt from the SiO_2, and 3% NaCl solution presents the greatest effect. In the asphalt-$CaCO_3$ system, the $CaCO_3$ thickness is 22.02 Å, and the asphalt molecules are embedded in $CaCO_3$ at dry. NaCl solution can replace the asphalt embedded in the $CaCO_3$, debonding the asphalt away from $CaCO_3$. The greater the NaCl concentration, the further the distance between asphalt and $CaCO_3$.

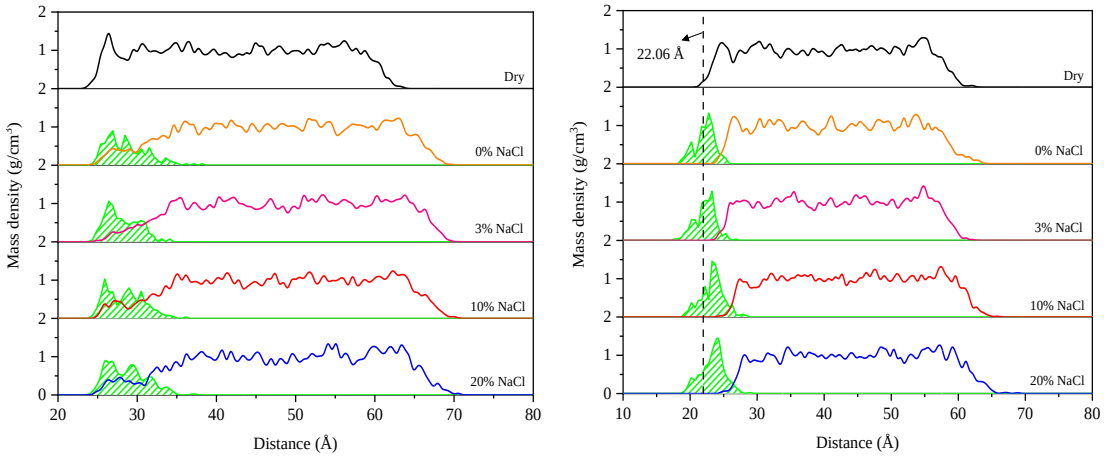

Fig. 9. Mass density of molecules towards the lengthwise direction (green area represents NaCl solution); (a) asphalt and NaCl solution in the asphalt-SiO_2 system; (b), asphalt and NaCl solution in the asphalt-$CaCO_3$ system.

3.4.2. Distribution of asphalt components

The spatial distribution of asphalt molecules is associated with the distribution of the four components. In the asphalt-SiO_2 system, the mass density of component molecules toward the lengthwise direction is illustrated in Fig. 10a to 10e. In the dry environment, the asphalt components agglomerate at the asphalt-mineral interface. And saturates have the greatest relative concentration, which is consistent with previous research findings [49]. This might be explained by the fact that the saturates are a non-polar component with relatively low molecular weight and weak intermolecular interactions, and diffusion potential resistance are minimal. The relative concentrations of aromatics and resins are lower than that of the saturates due to the lower mass fraction in asphalt molecular. Asphaltenes are polar but also have the highest molecular weight, and macromolecules are strongly hindered and repelled in asphalt, resulting in the lowest concentration [53]. The agglomeration of each component on the interface is weakened by 0% NaCl solution and 3% NaCl solution. Due to the decrease in D of the NaCl solution, the saturates with the lowest molecular weight agglomerate at the interface through 10% NaCl solution, while there is no obvious change in the distribution of the other components. The distribution concentration of saturates and resins further increases at the interface because of the further decline in D

of 20% NaCl solution. Because the resins are the most polar component of the asphalt components, the polarity is beneficial to the agglomeration of asphalt components on the SiO_2. It is known that the agglomeration of components is mainly affected by the D of the NaCl solution and the polarity of asphalt components, and the components agglomerated on the surface of SiO_2 in the NaCl environment are mainly saturates.

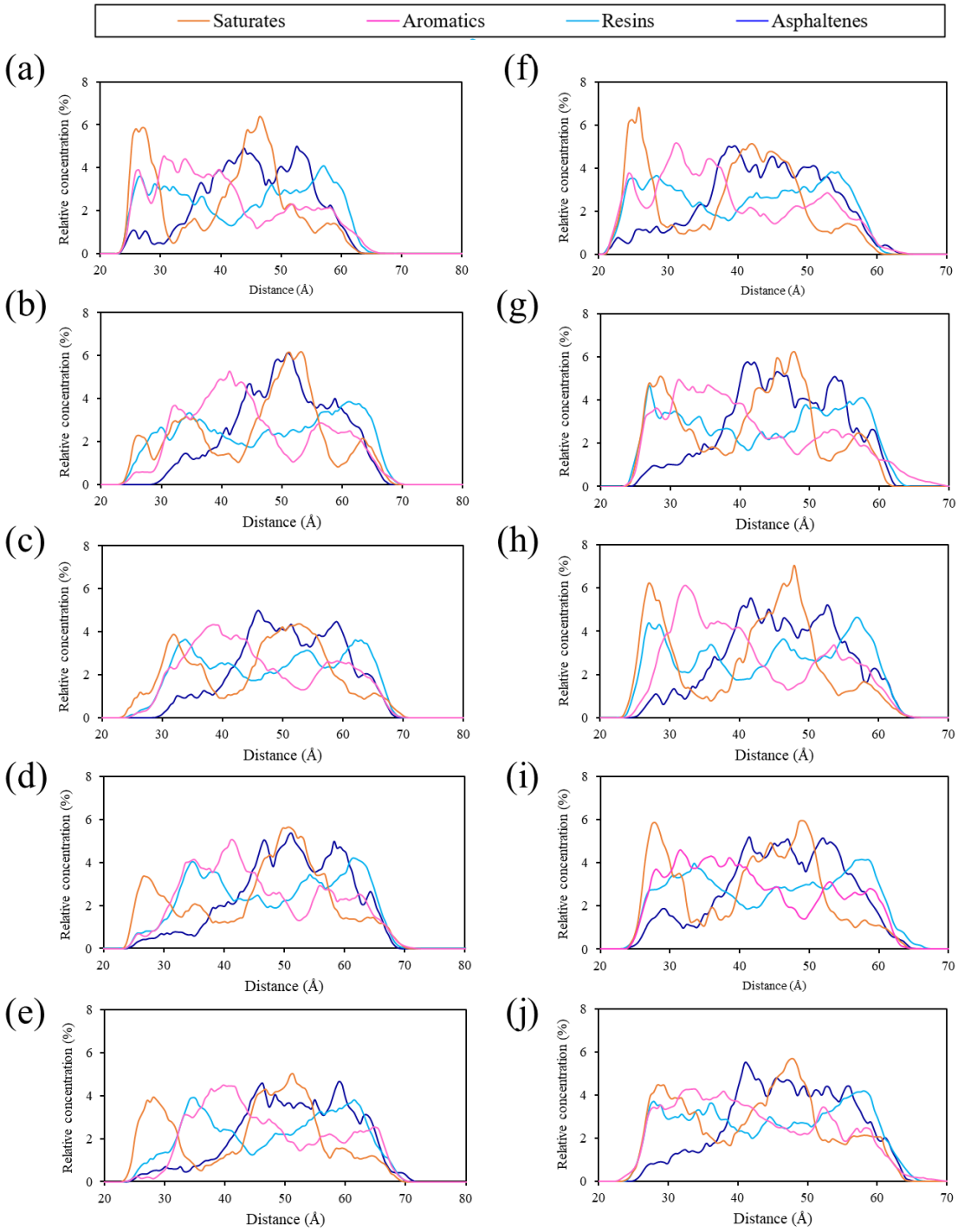

Fig. 10. Mass density of asphalt components towards lengthwise direction; (a), (b), (c), (d), and (e) asphalt-SiO_2 at dry, 0%, 3%, 10%, and 20% NaCl solution; (f), (g), (h), (i), and (j) asphalt-$CaCO_3$ at dry,

0%, 3%, 10%, and 20% NaCl solution.

In the asphalt-$CaCO_3$ system, the spatial distribution of asphalt components is shown in Fig. 10f to 10j. In the dry environment, the asphalt components were distributed at the interface in a consistent concentration as in the asphalt-SiO_2 system. In the 0% NaCl solution, all components move away from the interface. The agglomeration of the saturates at the interface was enhanced slightly by 3% NaCl, while it decreases the agglomeration of the other component. However, the agglomeration of all components is gradually weakened by 10% and 20 % NaCl. It manifests that the NaCl concentration has a negative influence on the distribution of the four components at the $CaCO_3$ interface.

3.4.3. Diffusion coefficient of asphalt components

The D of the asphalt components and the D of asphalt molecule in the system towards the mineral surface can describe the adhesion kinetic behavior between asphalt components and minerals. These indexes in the asphalt-SiO_2 system are depicted in Fig. 11a. The color intensity of the background plate corresponds to the D of asphalt molecule, which is convenient to observe the behavior of asphalt molecules more intuitively. Saturates and resins have the larger D at dry, followed by asphaltenes and aromatic. The D of all components increases at 0% NaCl solution. And the aromatics with the lowest molecular weight have the greatest D, followed by the polar components resins and asphaltenes, and the saturates have the minimum D. The cross-sectional D of 3% NaCl solution hinders the diffusion of all components except the saturates are reduced, in the order of saturates > aromatics > resins > asphaltenes. That can be because the saturates has a relatively low molecular weight with non-polar and weak intermolecular interactions and therefore diffuses more easily to the surface of SiO_2. And it is suggested that the diffusion of polar components towards the SiO_2 surface is inhibited by the polarization-inducing effect of low concentrations of Cl^- [25]. The diffusion of the components was facilitated by the decrease in cross-sectional D of the 10% and 20% NaCl solutions, with 10% NaCl contributing the most to the diffusion of the saturated fraction, and 20% contributing more to the other three components. The D of

asphaltenes is almost minimum in different environments, which is because asphaltenes have the highest molecular weight and the highest molecular resistance to movement. Therefore, the diffusion of the saturates is promoted to dominate the diffusion of asphalt at the interface in the NaCl environment, and it is promoted most by 10% NaCl. The diffusion of the other components decreases and then increases with increasing NaCl concentration, reaching a minimum at 3% NaCl.

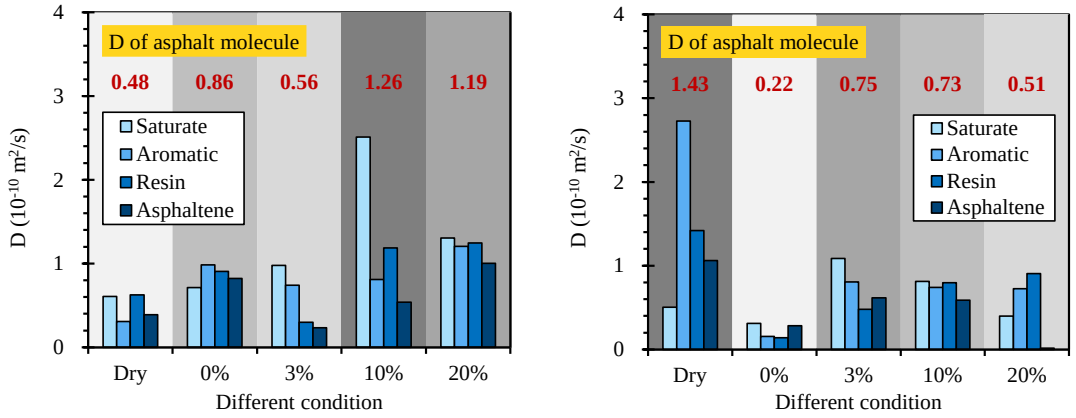

Fig. 11. Diffusion coefficient of asphalt components; (a) asphalt-SiO_2 system; (b) asphalt-$CaCO_3$ system.

From Fig. 11b, in the asphalt-$CaCO_3$ system, the aromatics have the larger D at dry, followed by polar components containing resins and asphaltenes, and the saturates have the smallest D. The order of polarity of asphalt components is the saturates, aromatics, asphaltenes, and resins. And resins and asphaltene as polar components are more adsorbed by the ionic bonding of $CaCO_3$. As a nonpolar component, the aromatics contain a benzene ring which gives the greater electron cloud density and dipole moment and has the smallest molecular weight and the smallest kinematic site resistance. These may be responsible for its maximum D under the ionic bonding of $CaCO_3$. The diffusion of all components is strongly limited by 0% NaCl solution, and the asphalt diffusion is dominated by saturates and asphaltenes. The diffusion of the components is slightly facilitated by 3% NaCl solution compared to 0% NaCl solution and the D values of the components are inversely proportional to the polarity. The 10% NaCl solution increases the D of the resins and decreases the D of the other components. This trend was further facilitated by the 20% NaCl solution and the D of the asphaltenes was close to 0. Thus, NaCl

facilitated the diffusion of all the components and the diffusion of the resins is increased as the increasing NaCl concentration, while the D of the other components reaches a maximum at 3% NaCl solution. That indicates that the resins are the most sensitive to NaCl in the asphalt-$CaCO_3$ interface, and its diffusion restricts the movement of the other components.

3.5. *Effect of NaCl solution on adhesion of asphalt-mineral interface*

3.5.1. Adhesion work between asphalt molecules and minerals

The adhesion work is used to evaluate the impact of NaCl solution on the adhesion property of the asphalt-mineral interface. The work required to separate the asphalt from the mineral at the interface is known as the adhesion work and it determines the resistance to separation at the interface [54]. The adhesion work of asphalt-mineral in NaCl environments was calculated by Eq. (7) [55].

$$W_{AM} = \frac{\Delta E_{AM}}{A} = \frac{E_A + E_M - E_{AM}}{A} \tag{7}$$

where W_{AM} and ΔE_{AM} express the adhesion work and interaction energy of asphalt-minerals, respectively; E_B, E_M, and E_{BM} express the potential energies of asphalt, mineral, and asphalt-mineral, respectively; and A expresses the area of contact between the asphalt and minerals, quantified using the Connolly area of the surface of the mineral. From Fig. 12a and 12b, the adhesion work of asphalt-SiO_2 is mainly controlled by the non-bonding energy generated by van der Waals forces, and the electrostatic interactions are negligible. This might be explained by the fact that there is no hydrogen bond between SiO_2 and asphalt from Fig. 7a. The adhesion work at dry is 58.72 mJ /m^2, which is close to the previously reported experimental data [56]. And the adhesion of asphalt to SiO_2 can be deteriorated by NaCl, and 3% NaCl solution has the most obvious effect. The adhesion work of asphalt-$CaCO_3$ is controlled by the non-bonding energy resulting from the interaction of electrostatic forces and van der Waals forces. The adhesion work provided by van der Waals forces is reduced by 76.43% by 0% NaCl solution, and the adhesion work provided by electrostatic forces is reduced to 1.03 mJ /m^2, resulting in a significant reduction in the interfacial adhesion work. This might be explained by the fact that the hydrogen bond

between the asphalt and $CaCO_3$ is replaced by the NaCl solution, and the adhesion work provided by the electrostatic force is almost 0. And the adhesion work generally decreases with NaCl concentration. The adhesion work is closely related to the agglomeration state of asphalt molecules at the mineral surface.

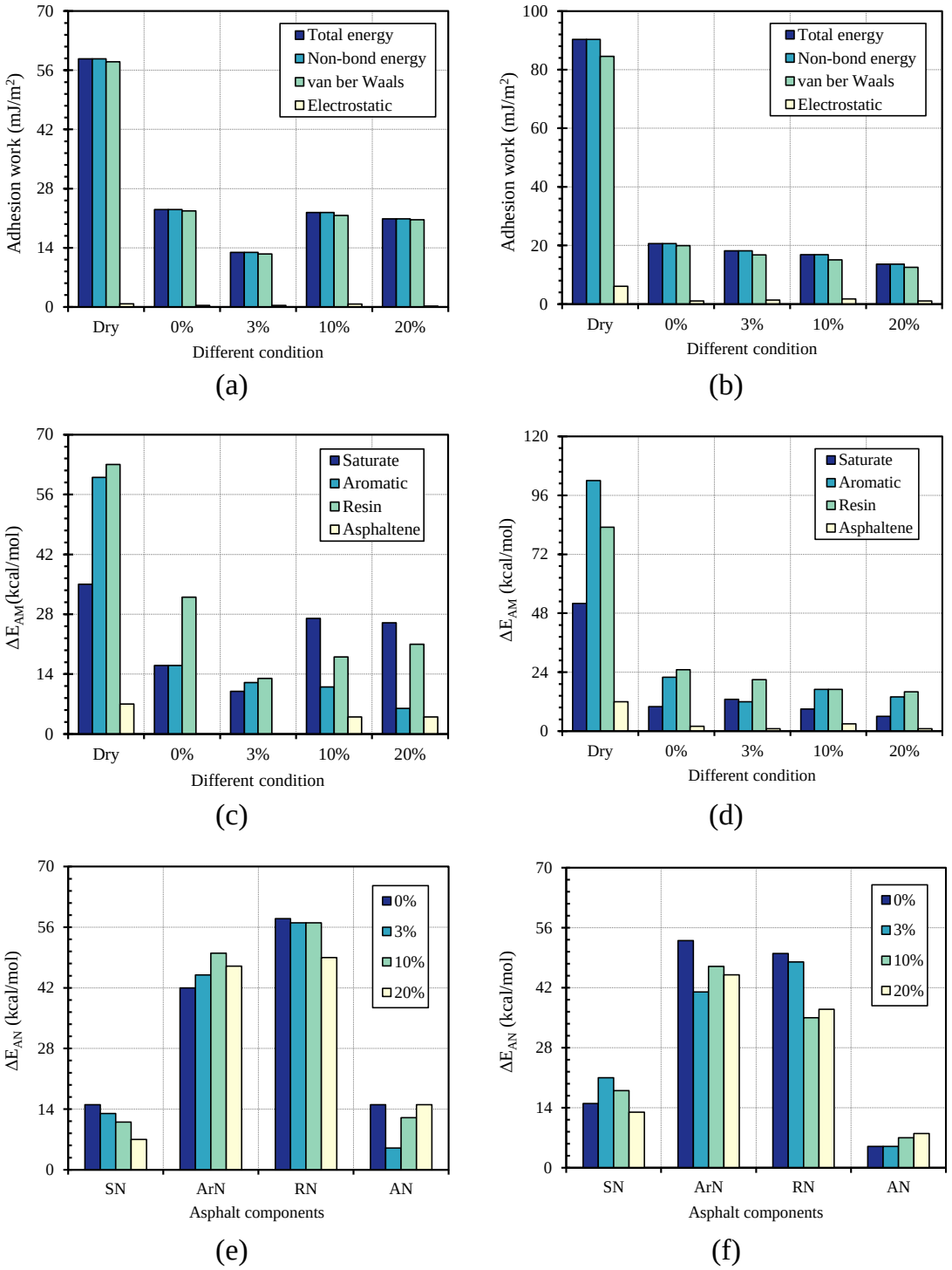

Fig. 12. Adhesion work and interaction energy in the asphalt-mineral system; (a) and (b) contribution of non-bonding energy for adhesion work in asphalt-SiO_2 and asphalt-$CaCO_3$; (c) and (d) interaction energy of asphalt components-SiO_2 and asphalt components-$CaCO_3$; (e) and (f) interaction energy of system

components-NaCl solution.

3.5.2. Interaction energy between asphalt components and minerals

The interaction energies between asphalt components and minerals were further analyzed to investigate the damage characteristic of adhesion work changing with NaCl concentration, as shown in Fig. 12c and 12d. In the asphalt-SiO_2 system, the ΔE_{AM} of resins and aromatics, which have the greater mass fraction, was greater, followed by saturates and asphaltenes at dry. The 0 % NaCl solution reduces the ΔE_{AM} of all components, among which the ΔE_{AM} of resins is the largest, and the ΔE_{AM} of asphaltene was close to 0 mJ /m^2. The ΔE_{AM} of all components are further reduced by 3% NaCl solution. Both 10% and 20% NaCl solutions enhance the ΔE_{AM} of saturates, resins, and asphaltenes, and weaken the ΔE_{AM} of aromatics. In the NaCl environment, the main components that provide the ΔE_{AM} for the asphalt-SiO_2 interface are saturates and resins. In the asphalt-$CaCO_3$ system, the aromatics provide the greatest ΔE_{AM} for the interface at dry, followed by the resins, saturates, and asphaltenes. With the increase of NaCl concentration, the ΔE_{AM} of all asphalt components decline in volatility, indicating that the polarization induction effect of NaCl has a negative effect on the interfacial adhesion.

3.5.3. Interaction energy between NaCl solution and asphalt components

The ΔE_{AM} between NaCl solution and asphalt components is characterized to investigate the stripping effect of NaCl solutions on asphalt components on mineral materials, as shown in Figure 12e and 12f. In the asphalt-SiO_2 system, the ΔE_{AM} of the non-polar saturates is small, and decreases with the increase of NaCl concentration. And NaCl increases the ΔE_{AM} of the aromatics, which may be due to the hydrogen bonding between NaCl solution and aromatics. The resins have the greatest ΔE_{AM} compared to the other components, but the ΔE_{AM} decreases with increasing NaCl concentration. NaCl weakens the ΔE_{AM} of asphaltenes, but the weakening effect decreases with the increase of NaCl concentration, which is related to the spatial distribution of asphaltenes. That indicates that NaCl can weaken the adhesion between asphalt and SiO_2 by hindering the aggregation of saturates, resins and asphaltenes on the surface of SiO_2, enhancing the interaction between aqueous solution and aromatics to strip the

aromatics from the surface of SiO_2. In the system of asphalt-$CaCO_3$, NaCl increases the ΔE_{AM} of saturates and asphaltenes, indicating that NaCl promotes aqueous solution to strip saturates and asphaltenes adhesion on the surface, and saturates is more sensitive to low concentrations of NaCl. The ΔE_{AM} of aromatics and resins are reduced by NaCl as they gradually move away from $CaCO_3$ from Fig. 9f-j.

3.6. Damage mechanism of NaCl solution to the adhesion of the asphalt-aggregate interface

Considering the above results, the NaCl environment can affect the distribution and diffusion of asphalt components and therefore reduce the asphalt-minerals adhesion. The schematic graph of the adhesion behavior of asphalt with minerals in a NaCl environment is shown in Fig. 13. For the asphalt-SiO_2 system, the polarity of the solution is enhanced by 3% NaCl, and there are more free ions to promote the cross-section diffusion of the solution. Combined with the polarity induction effect, it hindered the diffusion of other components except the saturates to the surface of SiO_2. This might be explained by the fact that the saturates with the relatively low molecular weight is a non-polar component, therefore the intermolecular interaction is weak, and the diffusion potential resistance is extremely small [57]. In addition, the adhesion work between asphalt and SiO_2 is generated by non-bond energy provided by the van der Waals force. The 3% NaCl prevents the accumulation of saturates, resins, and asphaltenes and strips the aromatics on the SiO_2 surface, thus weakening the adhesion between asphalt and SiO_2. At this time, the resins rather than the other components provide the maximum energy for the interface. However, with the increase of NaCl concentration, contact ion pairs gradually increase, resulting in a decrease in the R_g and FFV of the solution. Subsequently, the movement of atoms in the solution is limited, thus inhibiting the diffusion of the solution [58]. And the accumulation of asphalt components except for resins on SiO_2 will not be hindered on a large scale, and the diffusion and distribution of saturates are still dominant. Therefore, the adhesion work between asphalt and SiO_2 at 10% and 20% NaCl solution is greater than that at 3% NaCl solution, and the saturates are divided into the adhesion work at the interface

451 providing the maximum interaction energy.

452 For the asphalt-$CaCO_3$ system, there is an embedded locking effect, and the dense hydrogen bonds
453 between asphalt and $CaCO_3$ exist at dry due to the ion bonds in $CaCO_3$. The water can break the hydrogen
454 bond between $CaCO_3$ and asphalt and form hydrogen bonds with asphalt components. The evenly
455 distributed NaCl solution between asphalt molecules and $CaCO_3$ removes asphalt away from $CaCO_3$,
456 thus destroying the embedded locking effect between asphalt and $CaCO_3$. The polar effects of sodium
457 and chloride ions promote the cross-sectional and longitudinal diffusion of NaCl solution at the interface
458 and the diffusion of each component of asphalt. The adhesion work between asphalt and $CaCO_3$ is
459 generated by the non-bonding energy provided by van der Waals forces together with electrostatic forces,
460 as $CaCO_3$ consists of ionic bonds [59]. The 3% NaCl increases the interaction between the aqueous
461 solution and the saturates and asphaltenes to strip them from $CaCO_3$, and makes the aromatics and resins
462 far away from $CaCO_3$, which weakens the adhesion between $CaCO_3$ and asphalt. At the same time, the
463 resins provide the maximum interaction energy for interfacial adhesion. With the increase of NaCl
464 concentration, sodium ions can be attracted by negatively charged oxygen atoms on CO_3^{2-}, thus
465 occupying the active site on $CaCO_3$ more easily. That prevents the formation of contact ion pairs in NaCl
466 solution, and makes it easier for chloride ions to penetrate the asphalt molecule and asphalt components
467 to detached from $CaCO_3$. Therefore, the interface adhesion is continuously weakened with increasing
468 NaCl concentration, and the resins with greater polarity provide the greatest interaction energy for the
469 interface adhesion, which is consistent with the previous study [60].

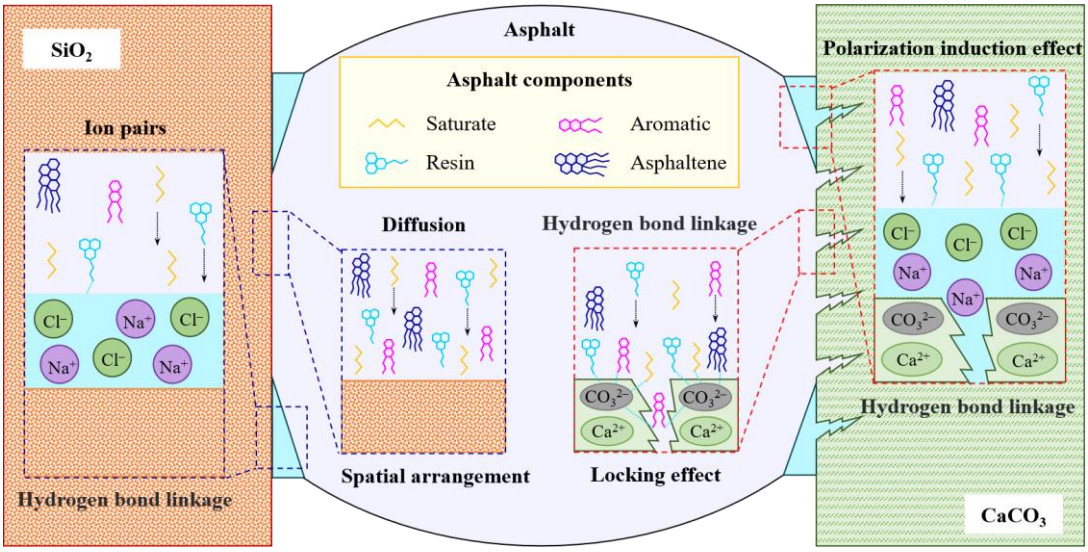

Fig. 13. Schematic graph of molecule migration model at asphalt-minerals interface.

4. Conclusions

In summary, the MD simulations of the asphalt-SiO_2 and asphalt-$CaCO_3$ interfaces were performed in an environment with extreme concentrations of NaCl, respectively. The characterizations contain the diffusion behavior of the NaCl solution at the interface, the spatial arrangement of asphalt components, and the changing trend of the interfacial adhesion work. It can be concluded that:

(1) As the NaCl concentration increases, the motion of atoms in the aqueous solution is restricted, which causes the 3% NaCl solution has the greatest D at the asphalt-SiO_2 interface and the asphalt-$CaCO_3$ interface.

(2) Due to the polarity caused by the ions, contact ion pairs exist abundantly in the NaCl solution, resulting in the self-aggregation of the NaCl solution at the asphalt-SiO_2 interface. In the asphalt-$CaCO_3$ system, the sodium ions are attracted to the negatively charged oxygen atoms on the CO_3^{2-}, readily occupying the active sites on the $CaCO_3$ surface. That prevents the formation of contact ion pairs in the NaCl solution and avoids self-aggregation of the NaCl solution, allowing the NaCl to cover the depressions on the $CaCO_3$ surface uniformly.

(3) The distribution and diffusion of asphalt components on the mineral surface are mainly affected by the D of NaCl solution and the polarity of asphalt components. And NaCl is conducive to

the formation of hydrogen bonds between water molecules and asphalt components.

(4) The 3% NaCl prevents the accumulation of saturates, resins, and asphaltenes on the SiO_2 surface, and strips aromatics from the SiO_2 surface, resulting in the maximum damage of interfacial adhesion work to the 55.93% of that in 0% NaCl solution. And the resins provide the maximum interaction energy. The adhesion work between asphalt and SiO_2 in 10% and 20% NaCl solution is greater than that in 3% NaCl solution. Among the four asphalt components, the saturates provide the greatest interaction energy for the interface.

(5) The 3% NaCl solution can strip saturates and asphaltenes from $CaCO_3$, keeping aromatics and resins away from $CaCO_3$. As the NaCl concentration increases, the chloride ions and asphaltenes move away from $CaCO_3$. The interfacial adhesion continued to diminish with increasing NaCl concentration, and the adhesion work is 66.03% of that at 20% NaCl solution. The resin with the highest polarity provides the largest interaction energy for interfacial adhesion.

This study exploits molecular dynamics to visualize the erosion process of the asphalt-aggregate interface by sodium chloride solution and explores the failure mechanism of interfacial adhesion. These findings provide new perspectives on the microscopic investigation of the interfacial adhesion behavior of asphalt mixture subjected to salt. The whole process of asphalt-aggregate interfacial separation in salt solution has not yet been visualized, considering the influence of factors such as solution surface tension. The effects of aging and temperature also need to be considered. Therefore, these topics are of interest to future research.

Credit author statement

Zou Yingxue: Conceptualization, Experiment, Writing-Original Draft. **Yangming Gao**: Methodology, Software, Writing-Review, Supervision. **Anqi Chen**: Writing Assistance, Supervision. **Shaopeng Wu**: Validation, Supervision. **Yuanyuan Li**: Writing-Review, Methodology. **Haiqin Xu**:

Software. **Huan Wang**: Methodology. **Ye Yang**: Data Curation. **Serji Amirkhanian**: Supervision.

Declaration of competing interest

The authors declare that they have no known competing financial interests or personal relationships that could have appeared to influence the work reported in this paper.

Acknowledgements

This work is financially supported by the National Natural Science Foundation of China [52208444]; the National Natural Science Foundation of China [52108416], the Hubei Province Supports Technological Innovation and Development Projects for High-Tech Enterprises [2021BAB074], the Hubei Science and Technology Innovation Talent and Service Project (International Science and Technology Cooperation) [2022EHB006], and the State Key Laboratory of Silicate Materials for Architectures (Wuhan University of Technology) [SYSJJ2022-21].

References

[1] Y. Meng, J. Lai, S. Mo, G. Fang, S. Deng, X. Wei, F. Yang, Investigating the deterioration mechanism of adhesion between asphalt and aggregate interface under acid rain erosion, Appl. Surf. Sci., 639 (2023) 158171.

[2] X. Gong, Q. Liu, H. Wang, P. Wan, S. Chen, J. Wu, S. Wu, Synthesis of environmental-curable CO2-based polyurethane and its enhancement on properties of asphalt binder, J. Clean. Prod., 384 (2023) 135576.

[3] A. Chen, Q. Deng, Y. Li, T. Bai, Z. Chen, J. Li, J. Feng, F. Wu, S. Wu, Q. Liu, Harmless treatment and environmentally friendly application of waste tires-TPCB/TPO composite-modified bitumen, Constr. Build. Mater., 325 (2022) 126785.

[4] Z. Liu, L. Sun, X. Gu, X. Wang, Q. Dong, Z. Zhou, J. Tang, Characteristics, mechanisms, and environmental LCA of WMA containing sasobit: An analysis perspective combing viscosity-temperature regression and interface bonding strength, J. Clean. Prod., 391 (2023) 136255.

[5] B. Cui, H. Wang, Oxidative aging mechanism of asphalt binder using experiment-derived average molecular model and ReaxFF molecular dynamics simulation, Fuel, 345 (2023) 128192.

[6] J. Li, J. Yu, S. Wu, J. Xie, The mechanical resistance of asphalt mixture with steel slag to deformation and skid degradation based on laboratory accelerated heavy loading test, Materials (Basel), 15 (3)(2022).

[7] J. Xie, J. Chen, L. Hu, S. Wu, Z. Wang, M. Li, C. Yang, Preparation, thermochromic properties and temperature controlling ability of novel pellets in ultra-thin wearing course, Constr. Build. Mater., 389 (2023) 131797.

[8] B. Cui, H. Wang, Molecular modeling of asphalt-aggregate debonding potential under moisture environment and interface defect, Appl. Surf. Sci., 606 (2022) 154858.

[9] X. Zhang, H. Chen, I. Hoff, The mutual effect and reaction mechanism of bitumen and de-icing salt solution, Constr. Build. Mater., 302 (2021) 124213.

[10] Y. Lv, S. Wu, N. Li, P. Cui, H. Wang, S. Amirkhanian, Z. Zhao, Performance and VOCs emission

548 inhibition of environmentally friendly rubber modified asphalt with UiO-66 MOFs, J. Clean. Prod., 385
549 (2023) 135633.
550 [11] B. Feng, H. Wang, S. Li, K. Ji, L. Li, R. Xiong, The durability of asphalt mixture with the action of
551 salt erosion: A review, Constr. Build. Mater., 315 (2022) 125749.
552 [12] X. Chen, D. Ren, G. Tian, J. Xu, R. Ali, C. Ai, Investigation on moisture damage resistance of
553 asphalt pavement in salt and acid erosion environments based on Multi-scale analysis, Constr. Build.
554 Mater., 366 (2023) 130177.
555 [13] O. Xu, X. Yang, S. Xiang, H. Zhang, Migration characteristic and model of chloride ions for NaCl-
556 based salt storage asphalt mixtures, Constr. Build. Mater., 280 (2021) 122482.
557 [14] Y. Zou, S. Amirkhanian, S. Xu, Y. Li, Y. Wang, J. Zhang, Effect of different aqueous solutions on
558 physicochemical properties of asphalt binder, Constr. Build. Mater., 286 (2021) 122810.
559 [15] R. Xiong, C. Chu, N. Qiao, L. Wang, F. Yang, Y. Sheng, B. Guan, D. Niu, J. Geng, H. Chen,
560 Performance evaluation of asphalt mixture exposed to dynamic water and chlorine salt erosion, Constr.
561 Build. Mater., 201 (2019) 121-126.
562 [16] Y. Zeng, Study on the influence of salt spray environment on the performance of asphalt mixture,
563 Dalian Jiaotong University, (2018).
564 [17] G. Qian, H. Yu, D. Jin, X. Bai, X. Gong, Different water environment coupled with ultraviolet
565 radiation on ageing of asphalt binder, Road Mater. Pavement, 22 (6)(2020) 1-14.
566 [18] C. Yang, S. Wu, J. Xie, S. Amirkhanian, Z. Zhao, H. Xu, F. Wang, L. Zhang, Development of
567 blending model for RAP and virgin asphalt in recycled asphalt mixtures via a micron-Fe3O4 tracer, J.
568 Clean. Prod., 383 (2023) 135407.
569 [19] O. Xu, S. Xiang, X. Yang, Y. Liu, Estimation of the surface free energy and moisture susceptibility
570 of asphalt mastic and aggregate system containing salt storage additive, Constr. Build. Mater., 318 (2022)
571 125814.
572 [20] K. Zhang, Y. Luo, W. Xie, J. Wu, Evaluation of road performance and adhesive characteristic of
573 asphalt binder in salt erosion environment, Mater. Today Commun., 25 (4)(2020) 101593.
574 [21] H. Yang, L. Pang, Y. Zou, Q. Liu, J. Xie, The effect of water solution erosion on rheological, cohesion
575 and adhesion properties of asphalt, Constr. Build. Mater., 246 (2020) 118465.
576 [22] S. Iliev, S. Tsibranska, A. Ivanova, S. Tcholakova, N. Denkov, Computational assessment of
577 hexadecane freezing by equilibrium atomistic molecular dynamics simulations, J. Colloid Interf. Sci.,
578 638 (2023) 743-757.
579 [23] M. Su, C. Si, Z. Zhang, H. Zhang, Molecular dynamics study on influence of Nano-ZnO/SBS on
580 physical properties and molecular structure of asphalt binder, Fuel, 263 (2020) 116777.
581 [24] Y. Hu, W. Si, X. Kang, Y. Xue, H. Wang, T. Parry, G.D. Airey, State of the art: Multiscale evaluation
582 of bitumen ageing behaviour, Fuel, 326 (2022) 125045.
583 [25] Z. Long, L. You, F. Xu, X. Tang, Y. Ding, A. Khanal, Y. Miao, Nanomechanical-atomistic insights
584 on interface interactions in asphalt mixtures with various chloride ion erosion statuses, J. Colloid Interf.
585 Sci., 628 (2022) 891-909.
586 [26] P. Chen, X. Luo, Y. Gao, Y. Zhang, Modeling percentages of cohesive and adhesive debonding in
587 bitumen-aggregate interfaces using molecular dynamics approaches, Appl. Surf. Sci., 571 (2022) 151318.
588 [27] C. Yang, S. Wu, P. Cui, S. Amirkhanian, Z. Zhao, F. Wang, L. Zhang, M. Wei, X. Zhou, J. Xie,
589 Performance characterization and enhancement mechanism of recycled asphalt mixtures involving high
590 RAP content and steel slag, J. Clean. Prod., 336 (2022) 130484.
591 [28] P. Cui, S. Wu, Y. Xiao, R. Hu, T. Yang, Environmental performance and functional analysis of chip
592 seals with recycled basic oxygen furnace slag as aggregate, J. Hazard. Mater., 405 (2021) 124441.
593 [29] Y. Deng, Q. Wu, Z. Li, X. Huang, S. Rao, Y. Liang, H. Lu, Crystal face dependent wettability of
594 alpha-quartz: Elucidation by time-of-flight secondary ion mass spectrometry techniques combined with
595 molecular dynamics, J. Colloid Interf. Sci., 607 (2022) 1699-1708.

[30] Y. Gao, Y. Zhang, Y. Yang, J. Zhang, F. Gu, Molecular dynamics investigation of interfacial adhesion between oxidised bitumen and mineral surfaces, Appl. Surf. Sci., 479 (2019) 449-462.
[31] D. Li, M. Greenfield, Chemical compositions of improved model asphalt systems for molecular simulations, Fuel, 115 (1)(2014) 347-356.
[32] Y. Gao, Y. Zhang, C. Zhang, X. Liu, R. Jing, Quantifying oxygen diffusion in bitumen films using molecular dynamics simulations, Constr. Build. Mater., 331 (2022) 127325.
[33] Z. Liu, X. Gu, X. Dong, B. Cui, D. Hu, Mechanism and performance of graphene modified asphalt: An experimental approach combined with molecular dynamic simulations, Case Stud. Constr. Mat., 18 (2023) e01749.
[34] Y. Gao, Y. Zhang, F. Gu, T. Xu, H. Wang, Impact of minerals and water on bitumen-mineral adhesion and debonding behaviours using molecular dynamics simulations, Constr. Build. Mater., 171 (2018) 214-222.
[35] S. Ren, X. Liu, P. Lin, Y. Gao, S. Erkens, Review on the diffusive and interfacial performance of bituminous materials: From a perspective of molecular dynamics simulation, J. Mol. Liq., 366 (2022) 120363.
[36] Y. Tang, Q. Meng, P. Ren, Spatial distribution and concentrations of salt fogs in a coastal urban environment: A case study in Zhuhai city, Build. Environ., 234 (2023) 110156.
[37] A.A. Khan, A.A. Razin, D.S.-S. Ahammed, M.S. Kaiser, Comparison of electrochemical corrosion performance of eutectic Al-Si automotive alloy in deep seawater and 3.5% NaCl solution, Mater. Today Proc., 82 (2023) 241-247.
[38] H. Yao, Q. Dai, Z. You, Molecular dynamics simulation of physicochemical properties of the asphalt model, Fuel, 164 (2016) 83-93.
[39] H. Zhang, M. Huang, J. Hong, F. Lai, Y. Gao, Molecular dynamics study on improvement effect of bis(2-hydroxyethyl) terephthalate on adhesive properties of asphalt-aggregate interface, Fuel, 285 (2021) 119175.
[40] D. Lesueur, The colloidal structure of bitumen: Consequences on the rheology and on the mechanisms of bitumen modification, Adv. Colloid Interfac., 145 (1-2)(2009) 42-82.
[41] P. Wang, Z. Dong, Y. Tan, Z. Liu, Investigating the interactions of the saturate, aromatic, resin, and asphaltene four fractions in asphalt binders by molecular simulations, Energy Fuels, 29 (1)(2015) 112-121.
[42] R. Li, Z. Leng, J. Yang, G. Lu, M. Huang, J. Lan, H. Zhang, Y. Bai, Z. Dong, Innovative application of waste polyethylene terephthalate (PET) derived additive as an antistripping agent for asphalt mixture: Experimental investigation and molecular dynamics simulation, Fuel, (2021) 300.
[43] W. Lu, Investigation of the interface structure and adhesion mchanism between asphalt and aggregate, Changan University, China, (2014).
[44] G. Li, Z. Chen, Y. Tan, X. Cong, Y. Dong, S. Xiao, Experimental and molecular dynamics simulation of hard asphalt microstructure, Constr. Build. Mater., 377 (2023) 131025.
[45] D. Hu, X. Gu, F. Yang, Z. Zhou, W. Bo, B. Cui, J. Pei, Atomic mechanisms of separation failure at the asphalt–aggregate interface and its dependence on aging and rejuvenation: Insights from molecular dynamics simulations and DFT calculations, Appl. Surf. Sci., 598 (2022) 153775.
[46] S. Alzobaidi, P. Wu, C. Da, X. Zhang, J. Hackbarth, T. Angeles, N.J. Rabat-Torki, S. MacAuliffe, S. Panja, K.P. Johnston, Effect of surface chemistry of silica nanoparticles on contact angle of oil on calcite surfaces in concentrated brine with divalent ions, J. Colloid Interf. Sci., 581 (2021) 656-668.
[47] C. He, B. Xu, X. Li, Effects of modified single-wall carbon nanotubes on the mechanical properties of polyvinyl alcohol composites by molecular dynamics simulation, Mater. Today Commun., 35 (2023) 105598.
[48] K. Shi, F. Ma, J. Liu, Z. Fu, R. Song, D. Yuan, C. Li, Rejuvenation effect of aged SBS-modified asphalt utilizing molecule analysis, J. Clean. Prod., 405 (2023) 136964.

[49] Long, X. Tang, Y. Ding, M. Miljković, A. Khanal, W. Ma, L. You, F. Xu, Influence of sea salt on the interfacial adhesion of bitumen–aggregate systems by molecular dynamics simulation, Constr. Build. Mater., 336 (2022) 127471.
[50] H. Chen, E. Ruckenstein, Hydrated Ions: From Individual Ions to Ion Pairs to Ion Clusters, J. Phys. Chem. B, 119 (39)(2015) 12671-12676.
[51] M.Z. Brela, Y. Didovets, M. Boczar, H. Sato, T. Nakajima, M.J. Wójcik, The hydrogen bond interaction dynamics in polyvinylphenol: Studied by Born-Oppenheimer molecular dynamics, Chem. Phys. Lett., 805 (2022) 139976.
[52] C. Liu, F. Min, L. Liu, J. Chen, Density functional theory study of water molecule adsorption on the α-quartz (001) surface with and without the presence of Na, ACS omega, 4 (7)(2019) 12711-12718.
[53] Eilers, H.J. J.phys.chem, The Colloidal Structure of Asphalt, J. Phys. Chem., 53 (8)(1949) 1195-1211.
[54] Z. Dong, Z. Liu, P. Wang, X. Gong, Nanostructure characterization of asphalt-aggregate interface through molecular dynamics simulation and atomic force microscopy, Fuel, 189 (2017) 155-163 155.
[55] F. Guo, J. Pei, G. Huang, J. Zhang, A. Cannone Falchetto, L. Korkiala-Tanttu, Investigation of the adhesion and debonding behaviors of rubber asphalt and aggregates using molecular dynamics simulation, Constr. Build. Mater., 371 (2023) 130781.
[56] A.E. Alvarez, E. Ovalles, S. Caro, Assessment of the effect of mineral filler on asphalt–aggregate interfaces based on thermodynamic properties, Constr. Build. Mater., 28 (1)(2012) 599-606.
[57] I.A. Wiehe, K.S. Liang, Asphaltenes, resins, and other petroleum macromolecules, Fluid Phase Equilibr., 117 (1-2)(1996) 201-210.
[58] J. Pliego, The role of intermolecular forces on ionic reactions: solvent effect, ion-pairing, aggregates and structured environment, Organic & Biomolecular Chemistry, 19 (9)(2021) 1900-1914.
[59] P. Feng, H. Wang, H. Ding, J. Xiao, M. Hassan, Effects of surface texture and its mineral composition on interfacial behavior between asphalt binder and coarse aggregate, Constr. Build. Mater., 262 (2020) 120869.
[60] W. Sun, H. Wang, Moisture effect on nanostructure and adhesion energy of asphalt on aggregate surface: A molecular dynamics study, Appl. Surf. Sci., 510 (2020) 145435.